Science Translational Medicine
AAAS

www.sciencetranslationalmedicine.org/cgi/content/full/10/464/eaat0150/DC1

Supplementary Materials for

Systems biology–based drug repositioning identifies digoxin as a potential therapy for groups 3 and 4 medulloblastoma

Lei Huang, Sarah Garrett Injac, Kemi Cui, Frank Braun, Qi Lin, Yuchen Du, Huiyuan Zhang, Mari Kogiso, Holly Lindsay, Sibo Zhao, Patricia Baxter, Adesina Adekunle, Tsz-Kwong Man, Hong Zhao, Xiao-Nan Li*, Ching C. Lau*, Stephen T. C. Wong*

*Corresponding author. Email: stwong@houstonmethodist.org (S.T.C.W.); clau@connecticutchildrens.org (C.C.L.); xiaonan@bcm.edu (X.-N.L.)

Published 24 October 2018, *Sci. Transl. Med.* **10**, eaat0150 (2018)
DOI: 10.1126/scitranslmed.aat0150

The PDF file includes:

Materials and Methods
Fig. S1. Cardiac glycosides do not inhibit the growth of the triple-negative breast cancer cell line MDA-MB231 in vitro.
Fig. S2. Establishment of ICb-2555MB, an orthotopic PDX model of group 3 MB.
Fig. S3. Assessment of long-surviving ICb-2555MB digoxin-treated mice for tumor formation.
Fig. S4. Digoxin plasma trough concentrations in tumor-bearing mice.
Fig. S5. Comparison of alternative single-agent digoxin treatment regimen with ionizing radiation alone in a group 3 model of MB.
Fig. S6. Comparison of a combination of digoxin and radiation with single-agent digoxin alone in a group 3 model of MB.
Fig. S7. Quality assessment of DFNs.
Table S1. Summary of patient data used to generate driver networks.
Table S6. Comparison of drug prediction performance between the two computational methods (DSNI-DFN versus CMAP-GSEA).
Table S9. Digoxin plasma trough concentrations in individual tumor-bearing mice.
Table S10. Thirty most differentially expressed genes after digoxin treatment of an orthotopic PDX model (ICb-2555MB) of group 3 MB.
Table S11. Thirty most differentially expressed genes after digoxin treatment of an orthotopic PDX model (ICb-1078MB) of group 4 MB.
References (*48*–*53*)

Other Supplementary Material for this manuscript includes the following:

(available at www.sciencetranslationalmedicine.org/cgi/content/full/10/464/eaat0150/DC1)

Table S2 (Microsoft Excel format). Driver genes that consist of somatic mutated genes, copy number variation genes, and differentially expressed genes in group 3 MB.
Table S3 (Microsoft Excel format). Driver genes that consist of somatic mutated genes, copy number variation genes, and differentially expressed genes in group 4 MB.
Table S4 (Microsoft Excel format). Identified driver signaling networks for group 3 MB.
Table S5 (Microsoft Excel format). Identified driver signaling networks for group 4 MB.
Table S7 (Microsoft Excel format). Ranking order of drugs in DSNI-DFN for group 3 MB.
Table S8 (Microsoft Excel format). Ranking order of drugs in CMAP-GSEA for group 3 MB.
Table S12 (Microsoft Excel format). Pathway enrichment analysis results using differentially expressed genes in digoxin-treated orthotopic PDX tumors of group 3 MB.
Table S13 (Microsoft Excel format). Pathway enrichment analysis results using differentially expressed genes in digoxin-treated orthotopic PDX tumors of group 4 MB.

Materials and Methods

Dysregulated driver network identification

We detected mutated genes by the applying Mutsig (*48*) to whole exome data of Group 3 (Group 4) MB. Gene copy number changes were detected by applying genomic identification of significant targets in cancer (GISTIC2) (*49*) to the single nucleotide polymorphisms (SNP) profiles of Group 3 (Group 4) MB. Differential expressed genes were analyzed by a Bayesian empirical test by comparing the gene expression data of Group 3 (Group 4) MB with SHH and WNT MB. Genes with mutations, copy number variations, or epigenetic (DNA methylation) modulations were designated as potential driver genes. Considering that not all gene mutations, gene copy number changes, or gene expression changes drive tumor growth, we evaluated the activities of gene-related pathways at the mRNA expression level. A NPBSA algorithm was used to derive driver signaling networks for subtype-specific MB (Figure 1A). The inputs of NPBSA are the predefined potential driver genes between subtype specific MB patients and control subjects. NPBSA was used to search each gene-involved subnetwork from an integrated human cancer signaling network (IHSCN), consisting of previously published human cancer signaling pathways (http://www.bri.nrc.ca/wang/) and our previous publication (*12*). The search started from every driver gene that formed an initial subnetwork with a single node. A subnetwork was defined as a gene set that induces a single connected component in IHSCN. The initial subnetwork grew into a final subnetwork after the searching process stopped. Certain driver genes that could not form a final subnetwork with two nodes were identified as false driver genes as they did not participate in activated signaling pathways.

NPBSA defines a network score (network activity) of a given subnetwork G on a Markov random field (formed by the gene sets of G) as: $NetS(G) = \frac{1}{m}\sum_{i\in S}\sqrt{\hat{\xi}_i} - \frac{\lambda}{n}\sum_{(i,k)\in E}\left(\frac{\hat{\xi}_i}{\sqrt{d_i}} - \frac{\hat{\xi}_k}{\sqrt{d_k}}\right)^2 - \frac{\gamma}{m}\sum_{i\in S}\left(Z_i - \hat{\xi}_i\right)^2/2$, where m is the number of genes in the subnetwork G, S is the gene set of G,E is the edge set that links genes from S and its nearest one neighbor, d_i is the degree of gene i in the IHCSN, $\boldsymbol{Z} = [Z_1, Z_2, \cdots, Z_m]^T$ is the Z-score of the genes, $\hat{\boldsymbol{\xi}} = [\hat{\xi}_1, \hat{\xi}_2, \cdots, \hat{\xi}_m]^T$ is the maximum posterior estimation of $\boldsymbol{Z}$. It applies simulated annealing to find a subnetwork G from IHCSN with the maximum network score, corresponding to a set of consistently up- (down-) regulated genes with significant p-values, a similar approach to that presented in Chen et al. (*50*).

Searching for subnetworks in NPBSA

In brief, given a driver gene g_0, considered as initial subnetwork G_0 with only one node, the z-score $\boldsymbol{Z}$ of the genes from IHCSN and a temperature T_0, the simulated annealing searching algorithm searched for a subnetwork from G_0, randomly sampled a new gene within two jumps of g_0 in IHCSN to get a new subnetwork $G_1 = \{g_0, g_1\}$, and computed the network score of $NetS(G_1)$. When no significant improvement of the network score was achieved, the simulated annealing stopped and a final subnetwork was output. Searching from different candidate driver genes will result in the identification of different driver signaling subnetworks for further evaluation. Given the potential for variation in the simulated annealing results due to noisy data, the heterogeneity of MB samples in the random sampling during the searching process and the

limited number of pediatric samples, we used a nonparametric bootstrapping strategy to compute the confidence level of the genes in the identified subnetwork. In the bootstrapping process, we randomly sampled from the mRNA (or methylation) profiling with replacement to generate a new dataset. We applied NPABSA on the new datasets. The confidence level of a given gene was computed as its frequency of appearance in detected subnetworks. The confidence score of gene j, $conf_j = \sum_{h=1}^{H} f(gene_j^h)/H$, h is the number of bootstrap repetitions, $f(gene_j^h)$ is 1 if gene j is selected in the h-*th* bootstrapping. A predefined threshold, 0.20, was used to select the genes with high confidence level, as genes appearing at high frequency will be more reliable.

Superimposition of drug-induced changes in gene expression onto dysregulated driver networks

A drug treatment transcriptional response matrix $\boldsymbol{X}(n \times m)$ was derived from the CMAP database for each drug in every cluster. Each column of $\boldsymbol{X}$, i.e., $\boldsymbol{X_i}$, is an n dimensional vector of gene fold-change (treatment vs. control) of drug i in the transcriptional response data; m is the number of drugs in a drug cluster; and n is the number of gene nodes in the group-specific MB driver signaling network. We used a Bayesian factor regression model (BFRM) to factorize the transcriptional response matrix into a series of underlying signatures using the model form $\boldsymbol{X_i} = \boldsymbol{A\lambda_i} + \boldsymbol{\varepsilon_i}(i = 1,2,\cdots,m)$. $\boldsymbol{A} = (\alpha_1, \alpha_2, \cdots, \alpha_k)$ is a sparse $n \times k$ matrix whose columns define the signatures $\boldsymbol{E_l}, l = 1,2,\cdots,k,$ and each numerical value $A_{j,l}$ defines the weight of gene j in the column of gene signature $\boldsymbol{E_l}$. $\boldsymbol{\varepsilon} = (\boldsymbol{\varepsilon}_1, \boldsymbol{\varepsilon}_2, \cdots, \boldsymbol{\varepsilon_m})$ and reflects the measurement error and the residual biological noise in the data. In addition, BFRM outputs a matrix $\boldsymbol{\rho} = (\boldsymbol{\rho}_1, \boldsymbol{\rho}_2, \cdots, \boldsymbol{\rho_k})$, which quantifies the probabilities of how each gene is associated with each factor $\boldsymbol{\lambda_i}$. To address

which networks are responsible for an unknown pharmacologic mechanism of a drug and to what extent they are related, we defined a weight matrix, $\boldsymbol{W}$ with $W_{ij} = A_{ij}$ if $\rho_{ij} > c$ and $W_{ij} = 0$ if $\rho_{ij} \leq c$, and an effect matrix$\boldsymbol{\lambda} = (\boldsymbol{\lambda_1}, \boldsymbol{\lambda_2}, \cdots, \boldsymbol{\lambda_m})$ with $\lambda_{k,i}$ quantifies the effect of drug i imposed on the gene signature, $\boldsymbol{E_k}$.

A drug-induced gene expression profile was defined based on $\boldsymbol{W}$ and $\boldsymbol{\lambda}$. We viewed the known and predicted drug-target interactions as physical drug-target interactions. We then defined the non-zero weights of the rows of the targets across signatures of drug d_i as a targetable signature set $\boldsymbol{ET_i}$. For each targetable signature $\boldsymbol{t} \in \boldsymbol{ET_i}$, we defined the product between $\mathcal{R}_t$ and the effect score $\lambda_{i,t}$ as the overall effect of drug d_i imposed on signature $\boldsymbol{t}$,$\eta_{i,t} = \mathcal{R}_t * \lambda_{i,t}$, where $\mathcal{R}_t = \sum_{j=1}^{n} W_{j,t}$ denotes the response of the signature $\boldsymbol{t}$ to the drug d_i. For a gene signature $\boldsymbol{t}$ that cannot be targeted by the drug d_i, i.e., the weights of the targets of drug d_i across the signature $\boldsymbol{t}$ are all 0, $\boldsymbol{t} \notin \boldsymbol{ET}_i$, $\eta_{i,t} = 0$. Therefore, for each driver signaling networkm_i, we obtained a drug-induced gene expression profile for the drug d_i , $\boldsymbol{\eta_{m_i d_i}} = (\eta_{g_{1m_i d_i}}, \eta_{g_{2m_i d_i}}, \cdots, \eta_{g_{km_i d_i}})$, $\{g_1, g_2, \cdots, g_k\}$ is the set of factors for network m_i.

Drug functional network reconstruction

Drug functional network reconstruction aims to identify drug communities that share common mechanisms of action. We reconstructed drug functional networks based on transcriptional data from the CMAP database, which contains 6,100 instances (1,309 compounds with different doses or on different cell lines). For each drug at each dose, genes were ranked based on their fold changes in response to treatment. Gene rank lists at different doses of the drug were merged

into one gene rank list by a hierarchical majority voting scheme (*12*). Subsequently, gene signatures for individual drugs were created by optimally selecting the top and bottom ranked genes according to their empirical distribution. The network-based gene set enrichment analysis (GSEA) score (*51*), $S_N(i,j)$, was used as the dissimilarity metric for the gene signatures between drug *i* and drug *j*. Edges were assigned among drugs whose dissimilarities are less than T, which is the third quantile of the empirical probability distribution of the drug dissimilarity, to obtain a drug functional network, N_G. The edge weakness of N_G was determined by the similarity $S_G(i,j)$, which is 1 - $S_N(i,j)$.

In addition, two different similarity metrics, the structural similarity, $S_s(i,j)$ and the high-throughput drug screening similarity, $S_h(i,j)$, were computed to obtain drug functional networks. $S_s(i,j)$ was defined by the Tanimoto 2D chemical similarity scores. $S_h(i,j)$ was the experimental/biochemical similarity of drugs and was extracted from the STITCH database (*23*). Two drug functional networks, N_s and N_h, were constructed by linking two drugs with similarity scores larger than a given threshold T (the third quantile of the empirical probability distribution of the drug similarity score) to obtain a drug-drug functional network. To avoid dealing with data collection bias and noise in different network data types, we used a network fusion algorithm (*11*) to integrate N_G,N_s and N_h into a drug functional network. During the fusion, edges with weak similarities disappeared and edges with strong similarities that existed in either one or two networks were added to the others. Weak similarities supported by the three networks were retained if their neighborhoods were tightly connected. Non-linear integration of network data allowed the network fusion algorithm to take advantage of the local structure, as well as common and complementary information in different network data types. The final drug functional network was clustered into drug functional clusters using a BNMβD method (*12*). We predicted

unknown drug-target interactions based on the known drug-target interactions within each drug cluster using a network recommendation algorithm that is described in our previous publication (*12*).

Construction of drug functional networks

Drug functional network reconstruction aims to identify groups of drugs that share common mechanisms of action. We independently reconstructed a drug functional network using transcriptional data from the CMAP database consisting of 6,100 data points (1,309 drugs or bioactive compounds with different doses or on different cell lines), the two-dimensional chemical structure information, and in vitro drug test data (*23*) between the 1,309 drugs. Drug functional networks with 1,309 nodes and 52,869 edges were clustered into 120 drug modules. Herein, the nodes of drug functional networks are drugs and edges represent the similarities between drugs. To evaluate the quality of these drug modules, we used two quantitative metrics, S_N and S_R that we previously introduced (*12*). Higher S_N and S_R values indicate more drugs in the same community sharing common targets. The average enrichment score, S_N, which is defined as $S_N = \frac{\sum_{i=1}^{N} s_i N_i}{\sum_{i=1}^{N} N_i}$, where $s_i = \frac{P_i}{N_i}$, P_i represents the number of drug pairs sharing targets in the i-th drug community, N_i is the number of drugs in that drug community, and N is the number of drug communities. A higher S_N value indicates more drugs in the same community sharing common targets. The second metric, S_R, is defined as the relative number of well-connected drug communities:$S_R = \frac{|\{s_i | s_i > d\}|}{N}$, where $\{s_i | s_i > d\}$ quantifies the number of well-connected drug communities, and d is a given threshold. We compared the quality of the identified drug cluster of our approach with a previously published one (*12*). A drug functional

network was reconstructed based only on the transcriptional responses from CMAP data in a previous work in which 106 drug functional modules were identified (*12*). Our method resulted in high-quality drug modules, which compared favorably to the previously reported approach, with an S_N of 0.746 vs. 0.583 and an S_R of 0.792 vs. 0.509 (fig. S7).

Drug repositioning based on specific dysregulated driver networks

For each identified driver signaling subnetwork, we calculated the mRNA fold-change signatures for Group 3 (or Group 4) MB patients using their average gene expression value minus the average value of control group (SHH and WNT MB). For drug repositioning purposes, we evaluated the targeted-effects of drugs on the identified driver signaling networks (subnetworks). A two-phase GSEA that is based on Kolmogorov-Smirnov statistics was applied to quantify the correlation of the targeted signatures of drug d_j with gene expression signatures of patients, $TE = \sum_{i=1}^{N} \left|\boldsymbol{\eta}_{m_i d_j}\right| ES\left(G_{m_i}, S_{d_j}\right)$. Here N is the number of driver signaling networks, $\left|\boldsymbol{\eta}_{m_i d_j}\right|$ is the norm of $\boldsymbol{\eta}_{m_i d_j}$ that indicates the targeting strength of drug d_j on the driver signaling network m_i, G_{m_i} is the gene expression fold change of disease on m_i, S_{d_j} is the gene expression fold change of drug d_j. We ranked all the drugs according to the correlation score TE, which characterizes the effects of drugs on the derived driver signaling networks.

Drug screening

Twenty thousand MED8A cells were seeded in duplicate in 96-well plates and incubated with 10μM Prestwick library drugs for 72h. There were 904 drugs that overlapped between the Prestwick library (1120 drugs) and CMAP (1,309 drugs or bioactive compounds). Cell viability

was assessed by a colorimetric method using CellTiter 96 Aqueous One Solution Cell Proliferation Assay kit (Promega).

In vitro evaluations of predicted cardiac glycoside drugs

Two MB cell lines, MED8A and D283, and a control triple negative breast cancer cell line, MDA-MB231-Br (a brain metastatic breast cancer cell line), were incubated with digoxigenin, digoxin, digitoxigenin, proscillaridin A and lanatoside C at concentrations ranging from $1\chi10^{-4}$ - 10^{2} μM in 0.01% DMSO (Sigma Aldrich) for 72 hours. Cell viability was then assessed by a colorimetric method using CellTiter 96 Aqueous One Solution Cell Proliferation Assay kit (Promega).

Patient-derived orthotopic xenograft models of MB

Animal studies on the orthotopic PDX mouse models of MB were conducted in accordance with the approval and the guidelines of Institutional Animal Care and Use Committee (IACUC) of Baylor College of Medicine. NOD.129S7 (B6)-*Rag1*^{tm1Mom}/J SCID mice (Jackson Lab, Bar Harbor, Maine) were utilized due to their ability to tolerate radiation with minimal toxicity compared to other strains of SCID mice. These mice were bred and maintained in a specific pathogen free animal facility of Texas Children's Hospital. The two orthotopic PDX models were established as we described previously. Intra-cerebellar orthotopic PDX (ICb-2555MB and ICb-1078MB) were established by direct injection of a surgical cannula into mouse cerebellum and maintenance of reproducible tumorigenicity was confirmed for more than 5 passages. Surgical transplantation of tumor cells into NOD/SCID mouse cerebellum was performed as

previously described. Mice of both sexes, aged 6–8 weeks, were anesthetized with isoflurane. Tumor cells (0.5×10^5) isolated from xenografts (ICb-2555MB in vivo passage 2 or ICb-1078MB in vivo passage 2 were suspended in 2 µL of culture medium and injected into the right cerebellar hemisphere via a 10-µL 26-gauge Hamilton Gastight 1701 syringe needle.

Determination of group status for ICb-2555MB by quantitative real-time PCR

Total RNA was extracted using TRIzol reagent (Invitrogen) from snap frozen tumor and normal tissue. cDNA synthesis from 1µg of total RNA was performed using High Capacity RNA-to-cDNA Kit (Applied Biosystems) following the manufacturer's protocol. Gene-specific quantitative RT-qPCR analysis was performed using SYBR Select Master Mix (Applied Biosystems) with a StepOnePlus Real-Time PCR system and MicroAmp Fast optical 96-well reaction plate (Applied Biosystems) using synthesized 5 ng cDNA. Expression of four genes were used for classification. The following primers were used including for the WNT group: *WIF1* (WNT inhibitory factor 1): Forward 5'-TGAATGGTGGACTTTGTGTGA, Reverse 5'-AGCAGGTGGTTGAGCAGTTT; for SHH group: *SFPR1* (secreted frizzled related protein 1) Forward 5'-AAGTGCAGGGAGGAAAAGTG, Reverse 5'-AAGACTGTGGGCAGAGAAGG; for Group 4: *KCNA1* (potassium voltage-gated channel subfamily A member 1) Forward 5'-CTGAGCAGGAAGGAAACCAG, Reverse 5'-CCTTAGAGTGGCGGGAGAG; for Group 3: *NPR3* (natriuretic peptide receptor 3) Forward 5'- AGAGTGGGGAGGAAAGAGGA, Reverse 5'-TAGTACGCACGGGGAGAAAG as well as for control: GAPDH Forward 5'-AAGGTGAAGGTCGGAGTCAA-3', Reverse 5'-AATGAAGGGGTCATTGATGG-3'. Relative mRNA expression was calculated using the $2^{-\Delta\Delta Ct}$ method and normalized against normal cerebral tissue expression. All quantitative RT-PCR assays were performed in triplicate.

Sub-classification of 2555MB expression pattern of known/representative samples for each MB group were included.

In vivo evaluations of digoxin therapy alone and in combination with radiation (XRT)

Implanted cells were allowed to grow for 17-24 days to form tumors, as our previous analysis on serial sections of whole mouse brains showed that the xenograft tumors often reach ~1-2 mm by 2 weeks and 3-5 mm by 4 weeks in size. For model ICb-2555MB, tumor-bearing mice were divided into 6 groups: untreated controls, digoxin intermittent (2 cycles of daily treatment for 14 days, separated by 21 days), digoxin continuous (daily 60 days), XRT only (2 Gy/day x 5 days to the craniospinal axis followed by 2 Gy/day for 5 days focal to the area of tumor injection), and intermittent digoxin combined with XRT. For model ICb-1078MB, only untreated controls and intermittent digoxin were tested. Clinical grade digoxin treatment (250 mcg/mL, West-Ward) 2mg/kg *i.p.* was initiated on day 24 for the intermittent groups and day 17 for continuous groups. Radiation therapy was initiated on day 17.

All mice were examined daily for signs of neurological deficits. At time of evidence of disease progression (such as neurological deficits or other evidence of physical decline such as loss of >20% body weight, decreased physical activity, or respiratory distress), the mice were euthanized and tumors were harvested and fixed in formalin for histological evaluation or cryo-preserved for potential molecular analysis and re-implantation. Two long-surviving mice in the ICb-1078MB treatment group were euthanized on post-implantation day 219 for tumor screening. Histologic evaluation of formalin fixed brains was carried out on 5 μm paraffin-embedded sections stained with hematoxylin and eosin.

Radiation of orthotopic PDX models

Radiation therapy was administered by fractionated radiation (64.5 cGy/sec for craniospinal irradiation, 105 cGy/sec for focal radiation) using the RS-2000 Biological irradiator (Rad Source Technologies). Mice in the radiation groups were sedated through inhaled isoflurane and irradiated 2 Gy daily (Craniospinal axis: 64.5 cGy/sec for 31 seconds) over 5 consecutive days followed by two days without treatment then further 2 Gy daily for 5 days (focal: 105 cGy/sec for 19 seconds).

X-rays were delivered to the xenograft tumors using custom made lead shields. For craniospinal radiation, an opening was designed which allowed for exposure of the whole brain and spine while protecting the rest of the body. Focal radiation was delivered via an opening designed to be ~2 mm larger in diameter than the expected size of intra-cerebellar xenograft tumors at the time of treatment.

Evaluation of digoxin trough concentrations

NOD/SCID mice were implanted with tumor cells from Icb-1078MB-rII as described above. The mice were observed until some showed signs of large tumor formation (for example, increased head size), at which time treatment was initiated with clinical grade digoxin as described above for 16 days. Twenty-four hours after the final digoxin dose, the mice were euthanized, and cardiac blood was drawn for analysis. Plasma digoxin testing was performed by Texas Children's Clinical Chemistry Laboratory using multi-point immuno-rate analysis.

RNA preparation and sequencing

Mice were implanted with tumor cells as described above. Mice were observed until they showed early signs of substantial tumor growth (for example, increased head size), at which time treatment with digoxin was initiated as described above. After 4 doses of digoxin, the mice were euthanized and tumors were frozen for further analysis. RNA was extracted from tumor cells using TRIzol reagent and mRNAs were selected using Poly (A) Purist MAG kit (Thermofisher). The RNA library prepared using NEBNext Ultra Directional RNA Library Prep Kit for Illumina (New England Biolabs, NEB) and sequenced using NextSeq 500/550 v2 Kits (high output 150 cycle, Illumina) on a HiSeq 2500 system.

RNA-seq reads were analyzed using FastQC for quality control. Then, short reads were aligned to the hg38 reference genome using TopHat (*52*) with default parameters. We counted the mapped reads to generate read counts for each gene using HTseq (*53*).

Immunohistochemical analysis

Mice were implanted with tumor cells as described above. For control and during treatment analysis, mice were observed until they showed early signs of substantial tumor growth (for example, increased head size). At that time mice were either euthanized (untreated controls) or treatment with digoxin was initiated as described above. After 4 doses of digoxin treatment, mice were euthanized. Harvested tumors were fixed in formalin and paraffin-embedded. Recurrent tumors were derived from survival studies described above. 5 μm paraffin-embedded tumor sections were stained using the EMD Millipore TUNEL Apoptosis Detection Kit per manufacturer's instructions.

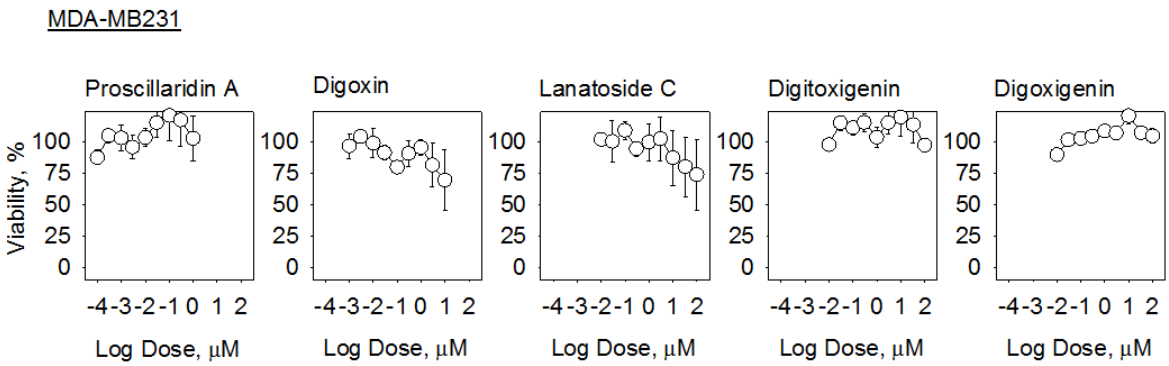

Fig. S1. Cardiac glycosides do not inhibit the growth of the triple-negative breast cancer cell line MDA-MB231 in vitro. The x-axis is the dose of a drug, the y-axis is the inhibition value on MDA-MB231 cell viability. There are 9 different dots in the dose-response curve for each drug indicates 9 different doses of that drug were tested. Cell viability was assessed at 72 hrs.

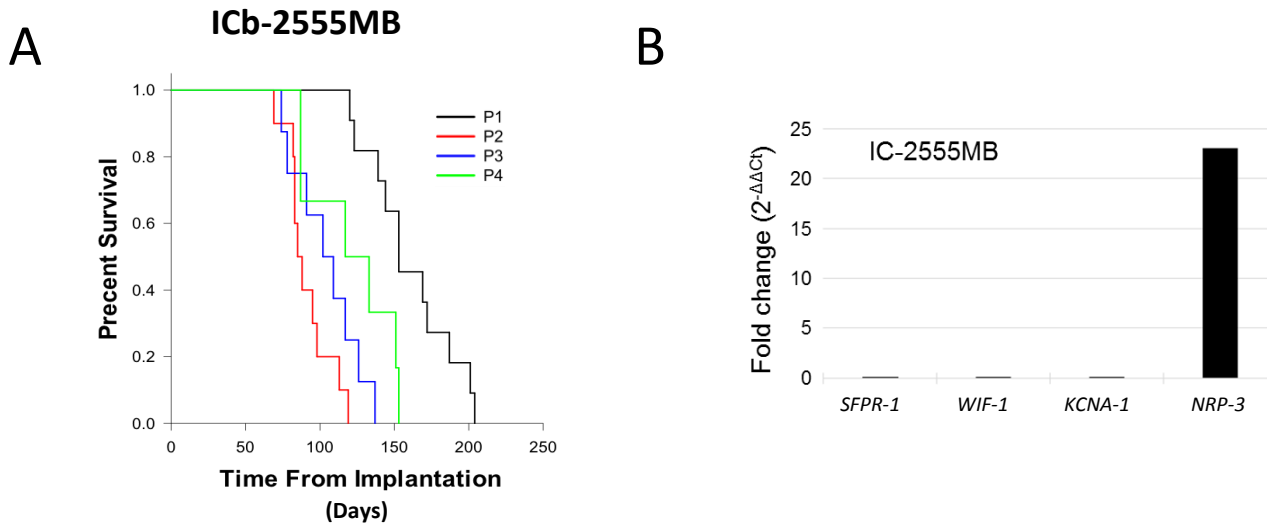

Fig. S2. Establishment of ICb-2555MB, an orthotopic PDX model of group 3 MB. (A) Kaplan-Meyer curve comparing xenograft passages for an orthotopic PDX model, ICb-2555MB. Tumor formation is preserved through multiple in vivo passages. (B) Expression of group 3 representative genes in 2555MB cells. Analysis of characteristic gene expression pattern for ICb-2555MB cells using subclass-specific genes (SHH-group: *SFPR-1*, WNT-group *WIF-1*, Group 4: *KCNA-1*, and Group 3: *NPR-3*). Expression is shown as fold change after normalization against *GAPDH* and normal tissue expression.

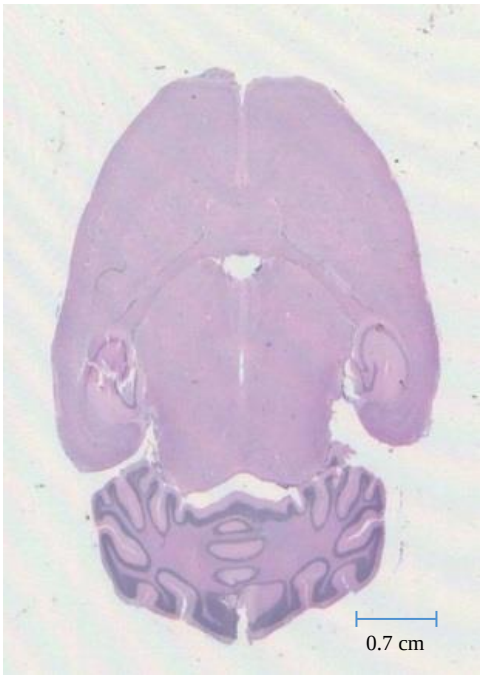

Fig. S3. Assessment of long-surviving ICb-2555MB digoxin-treated mice for tumor formation. H&E staining of brain from a Group 3 (ICb-2555MB) mouse which demonstrated prolonged survival after digoxin treatment with no evidence of a tumor. At the time of euthanasia, brains with no evidence of gross tumors were harvested and formalin fixed to assess for evidence of microscopic disease.

A

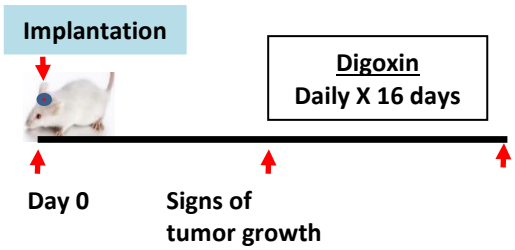

B

Digoxin Troughs	ng/mL
Clinical Goal Range	0.8-2
Highly Toxic	>10
Treated mouse average (n=6)	2.4 +/- 0.4

Fig. S4. Digoxin plasma trough concentrations in tumor-bearing mice. (A) Schematic of drug dosing experiments. (B) Average trough concentrations in digoxin-treated mice (2.4 ng/ml +/- 0.4) compared to target range for human patients (0.8-2 ng/ml).

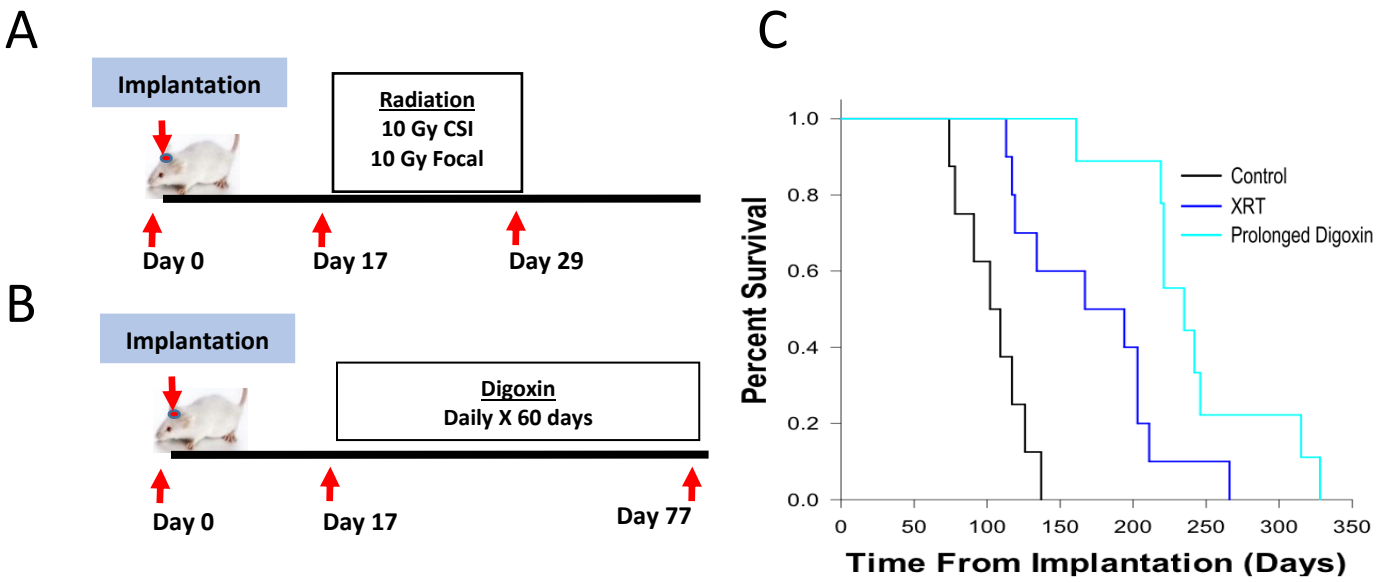

Fig. S5. Comparison of alternative single-agent digoxin treatment regimen with ionizing radiation alone in a group 3 model of MB. (A) Schematic for radiation treatment. 17 days after implantation of ICb-2555MB tumor cells, mice received fractionated radiation (2 Gy/day) to the craniospinal axis for 5 days. After allowing 2 days for recovery, they received an additional 2 Gy/day focal radiation to the posterior fossa for 5 days. (B) Schematic for prolonged digoxin treatment. 24 days after tumor cell implantation, treatment was initiated with digoxin (2mg/kg i.p. daily) for 60 days, after which the mice were observed. (C) Kaplan-Meyer curves comparing survival time in mice that received prolonged digoxin treatment (light blue, n=10) to those that received radiation alone (dark blue, n=10) and to untreated controls (black, n=8) in ICb-2555MB tumor bearing mice. Prolonged digoxin showed a statistically significant prolongation of survival (235 vs 167 days, log rank $p<0.01$) when compared with radiation therapy alone.

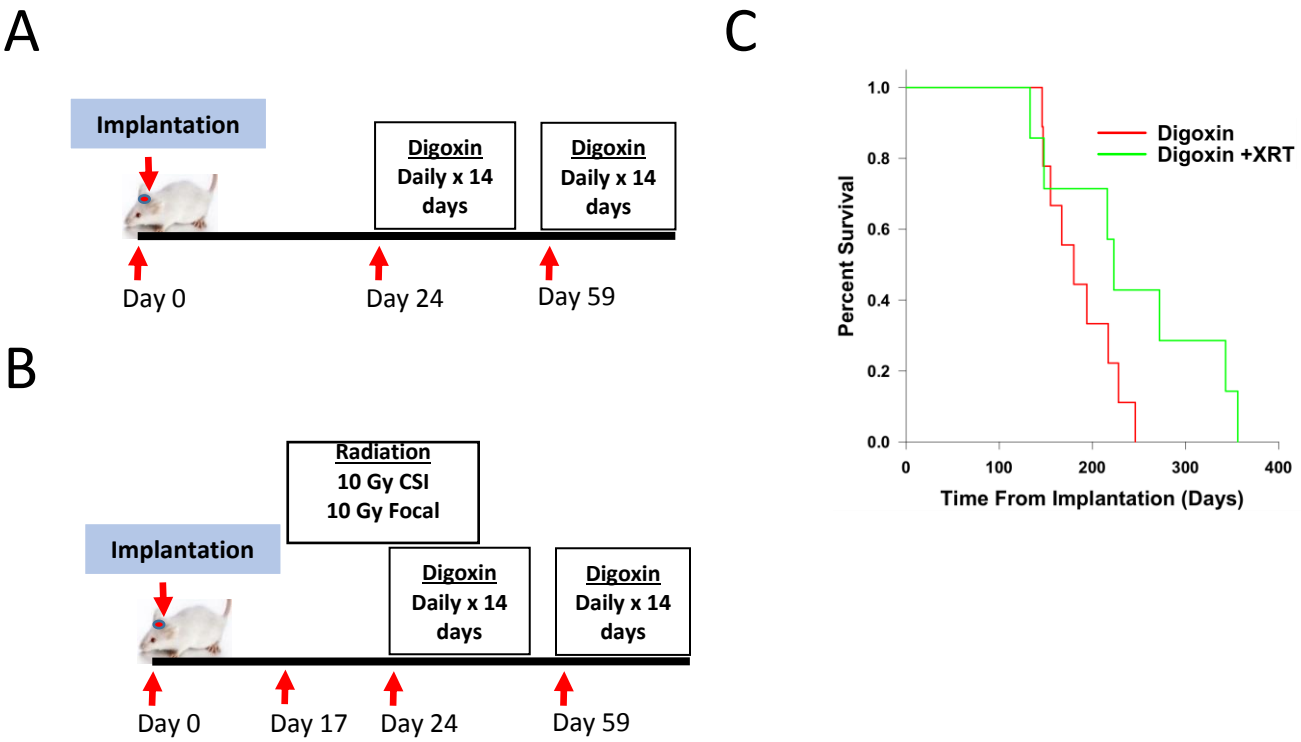

Fig. S6. Comparison of a combination of digoxin and radiation with single-agent digoxin alone in a group 3 model of MB. (A) Schematic for digoxin treatment. 24 days after implantation of ICb-2555MB tumor cells, mice received (2 mg/kg i.p. daily) for 14 days followed by a 21-day break then an additional 14 days of digoxin treatment. (B) Schematic for combination digoxin and radiation treatment. 17 days after tumor cell implantation the mice received fractionated radiation (2 Gy/day) to the craniospinal axis for 5 days. After allowing 2 days for recovery, they received an additional 2 Gy/day focal radiation to the posterior fossa for 5 days. Digoxin treatment was initiated 24 days after tumor cell implantation, received (2 mg/kg i.p. daily) for 14 days followed by a 21-day break then an additional 14 days of digoxin treatment after which the mice were observed. (C) Kaplan-Meyer curves comparing median survival time in mice that received single agent digoxin (red, n=10) to those that received combination digoxin and radiation (green, n=10). Combination therapy did not show significantly improved survival compared to digoxin alone (log rank, p=0.33).

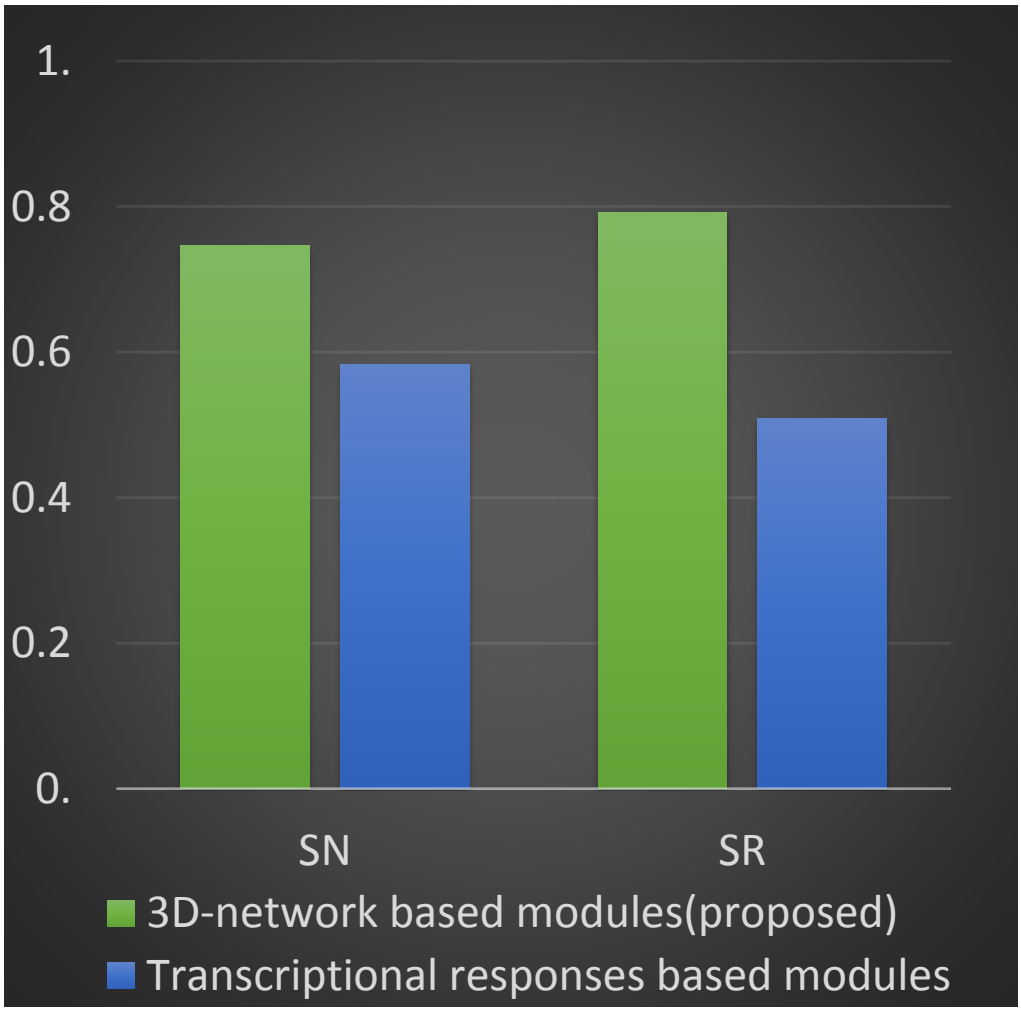

Fig. S7. Quality assessment of DFNs. Comparison of the proposed method for generating drug functional networks with transcriptional response-based approaches.

Table S1. Summary of patient data used to generate driver networks. Numbers indicate the number of patients evaluated for each data type. Control data refers to samples from patients with WNT or SHH group MBs to which the other samples were compared.

Data Type	Group 3 MB	Group 4 MB	Control	Data Source
mRNA expression	144	326	293	GSE85217
DNA copy number	316	261	Not applicable	GSE37384
DNA-seq	56	64	Not applicable	EGAS00001000215
DNA methylation	144	326	293	GSE85212

Table S6. Comparison of drug prediction performance between the two computational methods (DSNI-DFN versus CMAP-GSEA). Twelve out of the 100 top ranked drugs (12%) predicted by the DSNI-DFN method demonstrated >60% inhibition on cell viability of the group 3 MB cell line MED8A; only 4 out of the top ranked 100 drugs (4%) predicted by the CMAP-GSEA method showed >60% inhibition of cell viability of the same MED8A cells. Inhibition rate was calculated relative to the negative control:$1 - \frac{T-B}{C-B} * 100\%$,where C = OD490 value of the negative control well (mean value); T = OD490 value of the treated cells (mean value); B = OD490 value of the blank well (mean value).

	DSNI-DFN	In-vitro cell viability assay	CMAP-GSEA
	Rank	Inhibition rate (%)	Rank
digoxin	9	96.9	564
8-azaguanine	11	77.5	1108
camptothecin	12	62.3	1042
digitoxigenin	14	85.2	224
digoxigenin	27	99.1	14
lanatoside C	28	68.7	548
proscillaridin	34	100	49
daunorubicin	35	96.6	939
mitoxantrone	43	95.9	96

niclosamide	52	84.6	335
chlorambucil	76	69.9	1243
mesalazine	90	60.2	651

Table S9. Digoxin plasma trough concentrations in individual tumor-bearing mice. List of individual digoxin plasma trough values for 6 mice drawn 24 hours after the last digoxin treatment (2 mg/kg i.p.).

Sample #	Digoxin Trough (ng/mL)
1	2
2	2.5
3	2.4
4	2.1
5	2.3
6	3.1
Average	2.4 (SD +/- 0.4)

Table S10. Thirty most differentially expressed genes after digoxin treatment of an orthotopic PDX model (ICb-2555MB) of group 3 MB. The 15 most-upregulated and 15 most-downregulated genes were identified by comparing digoxin-treated with untreated RNA-seq profiles of Group 3 tumors. Genes were ranked by their log2 fold changes.

Genes	Log2 Fold change	Direction of expression change
LHX9	-3.06	down
ACBD6	-2.97	down
ADCYAP1	-2.54	down
DPYSL3	-1.95	down
STBD1	-1.89	down
CXCR4	-1.79	down
NDUFB9	-1.77	down
CSNK1D	-1.71	down
ARHGAP30	-1.60	down
NHLH2	-1.58	down
BOP1	-1.57	down
STMN2	-1.54	down
ABI2	-1.47	down
CYP19A1	-1.46	down

RBBP4	-1.43	down
FAM180A	3.49	up
ANXA13	3.40	up
PTER	2.83	up
FAM151A	2.44	up
LRBA	2.14	up
UQCC2	2.06	up
NQO2	1.84	up
ATP8B4	1.82	up
SLC8A1	1.76	up
ENDOV	1.75	up
RPTOR	1.71	up
ST3GAL6	1.70	up
CRYAB	1.67	up
FANCL	1.63	up
FAM179A	1.61	up

Table S11. Thirty most differentially expressed genes after digoxin treatment of an orthotopic PDX model (ICb-1078MB) of group 4 MB. The 15 most-upregulated and 15 most-downregulated genes identified by comparing digoxin-treated with untreated RNA-seq data of Group 4 tumors. Genes were ranked by their log2 fold changes.

Genes	Log2 Fold change	Direction of expression change
KCNA5	-4.71	down
KCNB2	-4.58	down
HK2	-4.36	down
GLT1D1	-4.22	down
FOXD2	-4.07	down
INF2	-4.04	down
TRABD	-3.96	down
RAB40A	-3.91	down
TTC36	-3.90	down
LBX1	-3.86	down
ZNF446	-3.81	down
PDE10A	-3.79	down
BACH1	-3.75	down
SLC26A6	-3.72	down

ST8SIA2	-3.71	down
FABP7	5.05	up
RDH12	4.76	up
TMEM63A	4.64	up
MFAP1	4.59	up
ARHGEF1	4.57	up
CTRB2	4.46	up
LACTB	4.43	up
TLE6	4.37	up
HIGD2A	4.26	up
SPAG4	4.16	up
LY75	4.12	up
IL12RB2	4.06	up
FER1L5	4.03	up
CELSR1	4.01	up
CENPBD1	4.01	up